New Two-Photon Activated Photodynamic Therapy Sensitizers Induce Xenograft Tumor Regressions after Near-IR Laser Treatment through the Body of the Host Mouse

Jean R. Starkey,[1] Aleksander K. Rebane,[2,6] Mikhail A. Drobizhev,[2] Fanqing Meng,[5] Aijun Gong,[5] Aleisha Elliott,[3] Kate McInnerney,[4] and Charles W. Spangler[5]

Abstract

Purpose: The aim of this study was to show that novel photodynamic therapy (PDT) sensitizers can be activated by two-photon absorption in the near-IR region of the spectrum and to show, for the first time, that such activation can lead to tumor regressions at significant tissue depth. These experiments also evaluated effects of high-energy femtosecond pulsed laser irradiation on normal tissues and characterized the response of xenograft tumors to our PDT protocols.

Experimental Design: Human small cell lung cancer (NCI-H69), non-small cell lung cancer (A549), and breast cancer (MDA-MB-231) xenografts were induced in *SCID* mice. Irradiation of sensitized tumors was undertaken through the bodies of tumor-bearing mice to give a treatment depth of 2 cm. Posttreatment tumor regressions and histopathology were carried out to determine the nature of the response to these new PDT agents. Microarray expression profiles were conducted to assess the similarity of responses to single and two-photon activated PDT.

Results: Regressions of all tumor types tested were seen. Histopathology was consistent with known PDT effects, and no, or minimal, changes were noted in irradiated normal tissues. Cluster analysis of microarray expression profiling showed reproducible changes in transcripts associated with apoptosis, stress, oxygen transport, and gene regulation.

Conclusions: These new PDT sensitizers can be used at a depth of 2 cm to produce excellent xenograft regressions. The tumor response was consistent with known responses to single-photon activated PDT. Experiments in larger animals are warranted to determine the maximal achievable depth of treatment.

Photodynamic therapy (PDT; ref. 1) is a protocol that uses light of the appropriate wavelength to activate photosensitizer accumulated in tumor tissue to its triplet state (2). The triplet excitation energy can be effectively transferred to molecular oxygen, resulting in the generation of singlet oxygen, superoxide radical, and other active oxygen species (2, 3). The singlet oxygen causes direct chemical damage to tumor and/or tumor endothelial cells (4), initiates a neutrophilic inflammatory response (5), and can stimulate both innate and specific antitumor immune responses (6–8). Singlet-oxygen production, however, requires a sufficiently high energy of the triplet state of the sensitizer. Long-wavelength near-IR (NIR) light $\lambda_{ex} > 750$ nm has relatively low-photon energy, which restricts the range of processes that can be activated by one-photon excitation. The relation between the wavelength and the minimum excitation energy of singlet oxygen is shown in Fig. 1A. The dark gray shaded area corresponds to the excitation energy below the required minimum value, $E_{so} < 1.5$ - 1.6 eV (9, 10), which shows that sensitization by one-photon absorption (1PA) fails in the phototherapeutic window 780 to 950 nm, where tissues have maximum transparency to light. Sensitization by simultaneous two-photon absorption (2PA; ref. 11) combines the energy of two photons and can provide sufficient energy for PDT in the phototherapeutic window. Because the intrinsic 2PA cross-sections of readily available sensitizers is very low, $\sigma_2 < 10$ to 100 Goeppert-Mayer units (where 1 Goeppert-Mayer unit = 10^{-50} cm^4 s photon^{-1}; ref. 12), there have been continuous efforts toward synthesizing new sensitizers with increased 2PA efficiency, including FRET dendrimers (13) and decorated nanoparticles (14). Recent *in vitro* studies with two-photon activation of Photofrin show killing of vascular endothelial cells but still require high-pulse energy and long illumination times (15). However, these authors concluded that sensitizers with two-photon cross-sections 2 to 3 orders of magnitude greater than that of Photofrin would be required for clinical efficacy. Two-photon activation of PDT

Authors' Affiliations: Departments of [1]Microbiology, [2]Physics, and [3]Chemistry and Biochemistry and [4]Genomics and Microdissection Facility, Montana State University; [5]MPA Technologies, Inc., Bozeman, Montana and [6]National Institute for Chemical Physics and Biophysics, Tallinn, Estonia

Received 9/11/07; revised 6/3/08; accepted 6/19/08.

Grant support: Montana Board for Research and Commercialization Technology (J.R. Starkey and C.W. Spangler), AFOSR FA9550-05-1-0357 (A.K. Rebane), and Office of Naval Research grant N00014-06-01-1016 (A.K. Rebane and J.R. Starkey).

The costs of publication of this article were defrayed in part by the payment of page charges. This article must therefore be hereby marked *advertisement* in accordance with 18 U.S.C. Section 1734 solely to indicate this fact.

Note: Supplementary data for this article are available at Clinical Cancer Research Online (http://clincancerres.aacrjournals.org/).

Requests for reprints: Jean R. Starkey, Department of Microbiology, Montana State University, 109 Lewis, Bozeman, MT 59717. Phone: 406-994-3962; Fax: 406-994-4926; E-mail: umbjs@montana.edu.

doi:10.1158/1078-0432.CCR-07-4162

Translational Relevance

Photodynamic therapy (PDT) is becoming increasingly popular as a versatile anticancer protocol. It can be used for drug-resistant tumors and in patients with conditions disallowing surgery. However, there is a pressing need for better exogenous PDT sensitizers. The poor depth efficacy of current sensitizers constitutes a major limitation and is directly related to the inferior tissue penetration of visible light, necessary for activation of currently approved compounds. A phototherapeutic window in the near IR (780-950 nm) permits deep tissue penetration but prohibits single-photon activation due to insufficient photon energy. We synthesized novel PDT sensitizers with high two-photon absorption cross-sections, allowing for effective activation in the phototherapeutic window. Our results, treating tumor xenografts through the bodies of *SCID* mice, showed robust regressions at depths of 2 cm. This warrants studies in larger animals, where we estimate maximal depth efficacy to lie somewhere between 5 and 7 cm. The use of two-photon activatable PDT sensitizers could greatly expand the types of human cancers that can be treated with PDT, in particular, providing new protocols for malignancies, such as small cell lung cancer, where modalities effective for multiply drug-resistant disease are urgently needed.

sensitizers allows for much greater precision in treatment as well as having a potential for significantly increased depth efficacy. The increased precision was recently shown *in vivo* for PDT-induced blood vessel closure (16). The current article seeks to show the increased depth efficacy possible with sensitizers designed for 2PA.

A limited number of PDT sensitizers have been approved for use as anticancer agents in several countries (1). Sensitizers may be exogenous (usually porphyrin, phthalocyanine, or chlorophyll derivatives) or endogenous following an injection of 5-amino-levulinic acid to drive a buildup of the active metabolite, protoporphyrin IX. PDT can be used in patients whose condition will not allow for surgery (17, 18) and in patients whose cancer has become drug resistant (19, 20). Healing is excellent with minimal scaring (1), and repeat treatments do not present problems (1). PDT is becoming increasingly popular as a versatile anticancer approach in the clinic. To date, insufficient experience precludes extensive use as a primary curative treatment (with the exception of Barrett's disease), but its potential for this is becoming increasingly obvious as experience is gained with adjuvant, palliative, and induction protocols.

There is a clear need for improvements in the design of exogenous PDT sensitizers. These compounds suffer from very limited depth efficacy, poor aqueous solubility, a tendency to aggregate in aqueous environments, and residual patient light sensitivity (2). Although the originally approved sensitizers, such as Photofrin and Foscan, show a limited preference for localization in tumor cells over normal cells, this does not provide much clinical advantage, and many groups are now investigating more effective methods of tumor and endothelial cell targeting (2, 20, 21). The utility of PDT is currently limited to topical, s.c., and endoscopic applications because the light typically used to generate singlet oxygen does not penetrate deeply into tissue (22). A phototherapeutic window exists between 780 and 950 nm, where tissues have relatively high transparency to light (Fig. 1A; ref. 2). On the short wavelength side, $\lambda < 780$ nm, the light is strongly attenuated by the UV-visible absorption of oxyhemoglobin as well as by scattering in skin and other tissues (Fig. 1A). On the long wavelength side, $\lambda > 950$ nm, the NIR absorption of water becomes strong. The achievable depth of light penetration increases steeply as the wavelength moves deeper into the phototherapeutic window. The increased penetration of longer wavelengths is currently exploited in fluorescence microscopy (23) as well as in NIR tomography, where breast penetration up to 100 mm depth has been shown (24). Furthermore, the increased depth of tissue penetration is accompanied by reduced heating and other detrimental side effects such as intrinsic phototoxicity. Tookad (Pd-bacteriopheophorbide; ref. 22) is the only sensitizer being used (experimentally) in man that exhibits a light absorbance wavelength, $\lambda = 763$ nm, close to the phototherapeutic window. However, no currently approved PDT agent can approach the potential 5 to 10 cm depth efficacy.

Given the difficulty of achieving 1PA singlet-oxygen activation in the NIR, we decided to design PDT sensitizers with high 2PA cross-sections. This allows us to study the activation of PDT well into the phototherapeutic window. To further improve the activity of our sensitizers, we also decided to use specific targeting to the somatostatin receptor type 2 (SST2r), which is overexpressed in several different human tumors (25). This article describes our initial experience with these novel sensitizers for experimental PDT of transplantable tumors in mice. In particular, we show effective PDT treatment at the maximal depth possible in mice.

Materials and Methods

Cell culture and xenograft induction. The human small cell lung cancer (SCLC) cell line NCI-H69, the human non-small cell lung cancer (NSCLC) cell line A549, the human breast carcinoma cell line MDA-MB-231, and the human pancreatic carcinoma cell line CAPAN-1 were all obtained from the American Type Culture Collection. The NCI-H69 (26) and MDA-MB-231 (27) cell lines overexpress the SST2r, whereas the A549 and CAPAN-1 cell lines do not express this receptor (28). Tumors from these cell lines were induced in CB/17 *SCID* mice. All cell lines were propagated in culture in DMEM/F-12 (Hyclone) supplemented with 10% fetal bovine serum (Mediatech), insulin, transferrin and selenium ITS (Mediatech), and cover antibiotics. CAPAN-1 cells were grown on laminin-1-coated tissue culture flasks. Incubation was carried out at 37°C in humidified air supplemented with 5% CO_2. A549 and MDA-MB-231 cells were harvested for tumor production when newly confluent employing a rinse with Ca^{2+}- and Mg^{2+}-free Tyrode's balanced saline followed by exposure to Ca^{2+}- and Mg^{2+}-free Tyrode's balanced saline containing 0.05% trypsin and 0.02% EDTA. As soon as the cells loosened from the substrate, they were harvested into complete, serum-containing medium to inactivate any remaining trypsin. The cells were centrifuged and resuspended in 2 mL Ca^{2+}- and Mg^{2+}-free Tyrode's balanced saline, and the cell numbers were adjusted to 10^7/mL. The NCI-H69 suspension line was harvested by pelleting the cells, resuspending them in Ca^{2+}- and Mg^{2+}-free Tyrode's balanced saline and passing the suspension through a stainless-steel mesh to filter out any remaining cell clumps. The cells were then adjusted to 10^7/mL. All tumors were induced by mixing 0.1 mL cell

suspension with 0.1 mL Matrigel solution and then injecting the mixture s.c. in the flank region (NCI-H69 and A549 cells) or the mammary fat pad (MDA-MB-231 cells). The recipient mice were monitored twice weekly until tumors were apparent. Tumors were used for PDT treatment when at least 0.8 cm diameter. Because a key aspect of this study was to show depth efficacy of treatment, mice bearing larger tumors were used. We were careful only to use animals that showed no evidence of metastatic disease, weight loss, tumor ulceration, or tumor interference with locomotion. Mice showing any of the above conditions were euthanized immediately. Age- and sex-matched *SCID* mice were obtained from the breeding colony at Montana State University Animal Resources Center. This colony was derived from animals obtained from The Jackson Laboratory. All mice were used at ages between 3 and 9 months, and all experiments using animals were approved by the Montana State University Institutional Animal Care and Use Committee. The Montana State University Animal Facility is an Association for Assessment and Accreditation of Laboratory Animal Care-approved facility.

Synthesis and spectra of the two-photon activatable photosensitizers. For this study, we used proprietary tetrapyrrole-based photosensitizers (US patent 6,953,570) with enhanced 2PA in NIR range of wavelengths. In its simplest implementation (29), the sensitizer incorporates a porphyrin core, with one or more 2PA-enhancing groups attached to the porphyrin *m*-positions by an ethynyl linker. On the remaining *m*-positions, groups that enhance intersystem crossing to an excited triplet state (usually 1-2,6-dichlorophenyl substituents) are incorporated without a linker group. Linking of the parent sensitizer to the tumor-targeting substituents is achieved via the 2,6-dichlorophenyl group in *p*-position. Figure 1B shows the structure of the targeted therapeutic complex used in the current studies. The parent sensitizer, MPA79, incorporates two 2PA-enhancing bis(diphenylamino)distyrylbenzene groups and two *p*-3-oxapropanoic acid functionalities. Two octreotate-targeting peptides, known SST2r and SST5r targeting agents (30, 31), are attached through ester links to the 3-oxapropanoic acid functionalities of the porphyrin core. Because the targeting unit is only weakly interacting with the MPA79 unit and does not absorb or emit light in visible-NIR range of wavelengths, its presence has only a minor effect on the photophysical properties of the complex.

The synthesis of all compounds was followed using nuclear magnetic resonance spectroscopy and UV-visible/IR spectroscopy, as appropriate. The therapeutic complex as well as the parent MPA79 photosensitizer were analyzed by matrix-assisted laser desorption ionization-time of flight spectroscopy at the Scripps Center for Mass Spectrometry. The mass spectra of both compounds indicated the expected molecular weights. The full synthetic scheme, reaction conditions, quantitative UV-visible spectral data, diagnostic nuclear magnetic resonance peaks, and matrix-assisted laser desorption ionization-time of flight mass spectra are provided in Supplementary Material.

The two-photon cross-section of the photosensitizer was measured in a separate set of experiments using a fluorescence excitation method. In this method, quadratic dependence of the fluorescence on the

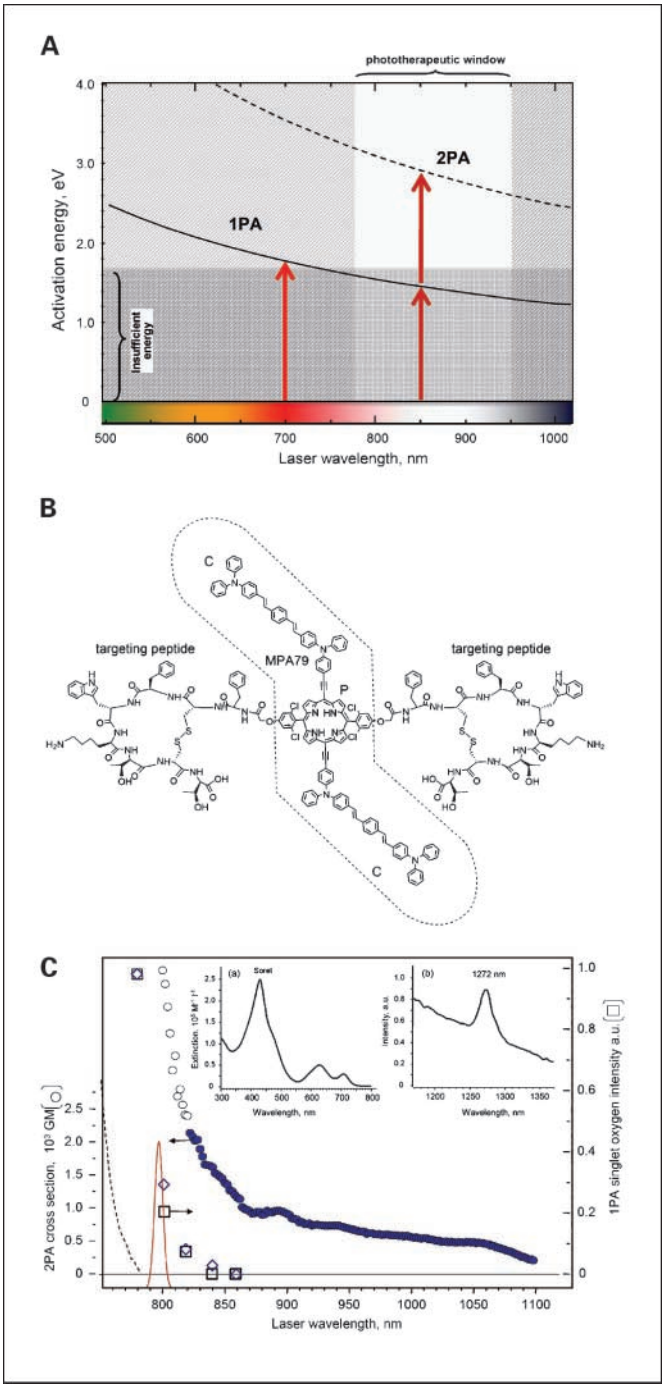

Fig. 1. Transparency characteristics of tissue (*A*) and its relationship to the spectroscopic characteristics of our novel sensitizer (*B* and *C*). *A,* relation between tissue transparency wavelength (*horizontal axes*) and absorbed energy (*vertical axes*). Energy below 1.5 to 1.6 eV (*dark gray shaded area*) is insufficient for singlet-oxygen generation via triplet-energy transfer. Wavelengths of low tissue transparency (*light grey shaded area*) are to the left and right sides of the phototherapeutic window 780 to 950 nm. The two curves show how the maximum absorbed energy depends on the wavelength. In the case of 1PA (*solid curve*), the relation is given by $E_{so} = hc\lambda^{-1}$, where *c* is velocity of light and *h* is Planck's constant. The 1PA curve misses the desired (*unshaded*) region. The relation for 2PA (*dashed curve*) is $E_{so} = 2hc\lambda^{-1}$, and the desired region can be achieved in its full length. *B,* structure of the therapeutic complex used in these experiments. The complex comprises two distinct parts: the singlet-oxygen generating unit, MPA79 (*inside dashed contour*), and the tumor-targeting unit, octreotate (*outside dashed contour*). The singlet-oxygen unit consists of the center porphyrin P and two covalently attached bis(diphenylamino)distyrylbenzene chromophores. *C, main figure,* femtosecond 2PA cross-section spectrum of MPA79 measured in methylene chloride using a fluorescence excitation method. In the laser wavelength range $\lambda_L = 820$ to 1,100 nm, the fluorescence showed purely quadratic dependence on the excitation pulse intensity (*filled circles*). At shorter wavelengths $\lambda_L < 820$ nm, the dependence showed an increasing linear component (*empty circles*). *Dashed line,* approximate shape of the long wavelength tail of the hot-band absorption, corresponding to the lowest energy transition in the linear absorption spectrum. Relative intensity of singlet-oxygen emission (*rectangles*) and fluorescence emission (*diamonds*) qualitatively follow a similar dependence on the excitation wavelength as the hot-band absorption. The red peak shows the spectrum of the treatment laser. *Inset a,* molar extinction spectrum of the targeted sensitizer in methylene chloride; *inset b,* singlet-oxygen luminescence spectrum at a constant excitation wavelength; *main figure,* singlet-oxygen emission intensity as a function of the excitation wavelength.

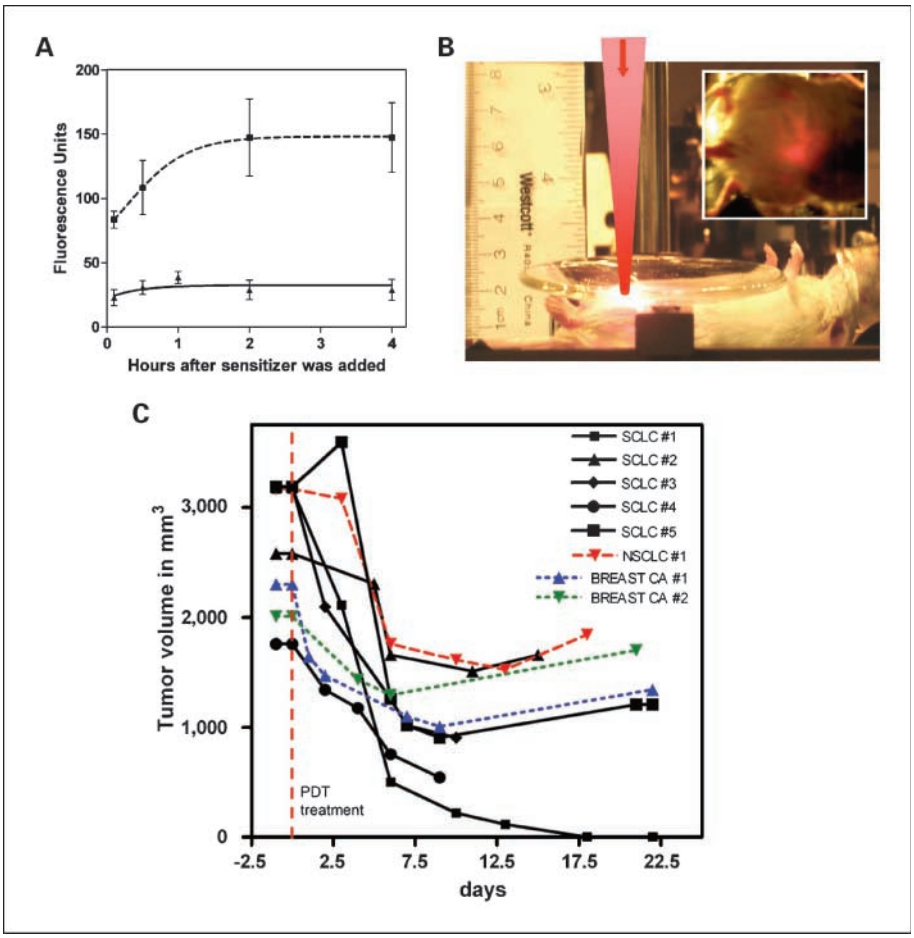

Fig. 2. PDT treatment xenografts using laser irradiation through the body of the host *SCID* mouse. *A,* uptake of targeted sensitizer by SST2r-positive MDA-MB-231 cells (*dashed line*) compared with SST2r-negative CAPAN-1 cells (*solid line*). The sensitizer was coupled to the NIR indotricarbocyanine fluor, and uptake was measured by quantitating the fluorescence of the washed cell monolayers with time as described in the text. *Y axis,* arbitrary fluorescence units for the entire cell monolayers after subtraction of the background. Mean ± SD of triplicate samples. A nonlinear curve fit was employed. *B,* a *SCID* mouse bearing a NCI-H69 SCLC xenograft receiving NIR laser activation. The watch glass on the ventral side of the mouse ensures a good optical interface between the laser beam and the mouse, and the addition of a few drops of glycerol at the interface also aids heat dissipation at the skin surface. *Inset,* laser light emanating from the tumor on the dorsal flank region of the mouse. *C,* PDT-induced regressions of NCI-H69 SCLC (*solid line*), A549 NSCLC (*red dashed line*), and MDA-MB-231 human breast cancer (*green* and *blue dashed lines*) xenografts in *SCID* mice.

excitation pulse intensity indicates simultaneous (intrinsic) 2PA, whereas linear dependence indicates 1PA. Figure 1C shows the linear and nonlinear spectroscopic properties of MPA79, the singlet oxygen generating porphyrin structure (see figure caption for explanation). The 2PA cross-section results are given in Goeppert-Mayer units.

To set up an appropriate treatment protocol, we first determined the time course for uptake of the targeted sensitizer. Because the fluorescence of the porphyrin in our sensitizer is quenched in aqueous solution, we used a modified version of the nanocomplex where one of the octreotate peptides was replaced with the NIR fluor; indotricarbocyanine (see Supplementary Materials for more information). The CAPAN-1 SST2r-negative and MDA-MB-231 SST2r-positive cell lines were grown in individual sides of two-chambered LabTek coverglass culture systems. When both cell types were newly confluent, the growth medium was removed and the cultures were washed three times with serum and phenol red-free DMEM/F-12. The targeted sensitizer was then added to the cultures using a ratio of sensitizer in HS-15 Solutol excipient (BASF) to serum and phenol red-free medium of 1.0:3.5, and the cultures were returned to the incubator. Immediately after sensitizer addition and at set times thereafter, the medium was removed from triplicate cultures. These were then washed three times with serum and phenol red-free medium before being scanned on the Kodak 2000MM instrument for the NIR fluorescence of the cell sheet.

PDT treatment of tumors. Solid sensitizer (1 mg; targeted therapeutic complex) was added to each of several 1.5 mL sterile microfuge tubes, and 0.3 mL liquid HS-15 at 40°C was added to each tube. These were then incubated at 40°C overnight in the dark. The tubes were then vortexed to complete mixing and centrifuged at 15,000 rpm for 5 min at room temperature. The dissolved sensitizer was then harvested, and all dissolved sensitizer aliquots were pooled and stored at ˉ20°C until use. Immediately before injection, the sensitizer in HS-15 was slowly mixed with warm serum-free DMEM/F-12. The sensitizer remained well dissolved in the HS-15 excipient even with extensive dilution with the aqueous DMEM/F-12. A therapeutic dose, however, cannot be delivered by i.v. injection because of the volume limitations imposed on i.v. injections in the mouse, coupled with the fact that the viscosity of HS-15 is too great to flow through the tail vein at the required concentration of this excipient. Therefore, tumors were sensitized using local infiltration of the tumor. The day before PDT treatment, the area over the tumor was depilated with Nair to remove overlying hair, which would otherwise scatter laser light during treatment. A 50% sensitizer solution in HS-15/serum-free medium (v/v) was slowly infiltrated into the tumor using no more than 0.2 mL volume. A warmed glass 1.0 mL luer lock tuberculin syringe and a 25-gauge needle were employed. The dose of sensitizer varied between 100 and 200 μg depending on the size of the tumor.

Figure 2A shows the time course for the uptake of the sensitizer by SST2r-positive tumor cells in tissue culture. Following these data, the mice were irradiated 4 h after the sensitizer infiltration. Femtosecond pulsed laser light at λ = 800 nm was used to activate the sensitizer. A cartoon of the experimental setup for PDT treatment of tumor-bearing mice is available in Supplementary Materials. The laser used was a 1 kHz repetition rate regenerative Ti:sapphire amplifier (Coherent Legend) seeded by a femtosecond oscillator (Coherent Mira 900). The light delivery system consisted of mirrors, an electronically operated shutter (Uniblitz) and focusing lens (f = 350 mm). The mouse was anesthetized with isofluorane in oxygen and positioned on a *x-y*

Table 1. Real-time quantitative PCR measurement of gene expression in control and PDT-treated NCI-H69 xenografts (β-actin as comparator transcript)

Expressed gene	Fold increase (PDT treated over control)	Mean comparative message concentration in control tumors*	Mean comparative message concentration in treated tumors*
HSP70	8.93	0.0177 ± 0.013	0.158 ± 0.014
Vascular endothelial growth factor	1.72	0.0272 ± 0.0085	0.0467 ± 0.00028
Hbα2 human primers	5.43	0.0234 ± 0.0078	0.127 ± 0.026
Hbα2 mouse primers	5.85	0.0706 ± 0.0092	0.413 ± 0.12
Bax	None	0.00188 ± 0.0019	0.00185 ± 0.00099
Bcl-2	None	0.0279 ± 0.0017	0.0246 ± 0.000071
Fos	2.00	0.0165 ± 0.0033	0.0329 ± 0.0062
Fas	3.50	$0.0988 \times 10^{-4} \pm 0.017 \times 10^{-4}$	$0.0348 \times 10^{-3} \pm 0.00007 \times 10^{-3}$

	Product size (bp)	Forward primer nucleotide sequence	Reverse primer nucleotide sequence
β-Actin	233	5′-GGACTTCGAGCAAGAGATGG-3′	5′-AGCACTGTGTTGGCGTACAG-3′
HSP70	229	5′-CCAAGCAGACCCAGACTTTC-3′	5′-GCCTTACCTGTGCTCCTGTC-3′
Vascular endothelial growth factor	173	5′-CCCACTGAGGAGTCCAACAT-3′	5′-AAATGCTTTCTCCGCTCTGA-3′
Hbα2 human primers	196	5′-CAAGACCTACTTCCCGCACT-3′	5′-GCAGTGGCTTAGGAGCTTGA-3′
Hbα2 mouse primers	153	5′-GTGCTCTCTGGGGAAGACAA-3′	5′-GCCGTGGCTTACATCAAAGT-3′
Bax	487	5′-GTTTCATCCAGGATCGAGCAG-3′	5′-CATCTTCTTCCAGATGGTGA-3′
Bcl-2	127	5′-CCTGTGGATGACTGAGTACC-3′	5′-GAGACAGCCAGGAGAAATCA-3′
Fos	233	5′-CCAACCTGCTGAAGGAGAAG-3′	5′-GCTGCTGATGCTCTTGACAG-3′
Fas	126	5′-MAGAAGGGRAGGAGTACA-3′	5′-TGCACTTGGTATTCTGGGTC-3′

Abbreviations: M, A/C; R, G/A.

motorized translation stage (Prior) controlled via a PC computer interface. A clear plastic plate was used as a support for the anesthetized mouse, which allowed the transmitted light intensity to be measured, and also the transmitted scattered light to be imaged with a digital camera. The laser beam spot size was adjusted by moving the focusing lens in a vertical *z*-direction. During the irradiation, a PC-controlled routine was used to move the mouse in a *x*-*y* raster pattern relative to the beam spot. Typical irradiation areas were 15 × 15 mm^2 and the distance between neighboring spots was 1 mm, whereas the diameter of the laser spot on the proximal surface of the animal was not less than 2 to 3 mm. The irradiation time at each spot was 5 s and the total irradiation times were 20 to 30 min. Thermal damage to the skin was avoided by (*a*) the rastering of the laser spot and (*b*) by using a watch glass laid on top of the mouse with glycerin contact fluid between the mouse skin and the watch glass. The average power of the laser at the skin level was 600 to 800 mW. The average irradiance was 10 to 20 W cm^{-2}, and the pulse duration at the skin was 150 to 200 fs. The energy per pulse was 0.6 to 0.8 mJ, and a corresponding peak irradiance was 10 to 100 GW cm^{-2}. The average power transmitted through the mouse was measured with a thermoelectric optical energy meter (Coherent, LabMaster) and was 60 to 80 mW, indicating that 10% of the laser energy passed through both the mouse (17 mm) and the tumor without being absorbed or scattered out of the field of interest.

Quantitation of the regression response of tumors to PDT treatment. The mice were closely monitored for the first 2 h after treatment and then twice daily for the first 2 days after treatment. After PDT treatment, the tumors were measured in three dimensions every other day. The tumor volume was determined using the formula for the volume of an ellipsoid.

Histopathology of treated and control tumors. Tumor, lung, liver, kidney, intestine, and skin tissue samples were harvested from treated and untreated control mice and fixed in 10% phosphate-buffered formalin. The tissue samples were processed for paraffin sections and stained with H&E. Tissue samples were evaluated at 0, 12, 24, and 48 h after treatment. In some cases, tumor tissues were marked with colored dye before fixing, so that their orientation, relative to the laser beam, could be determined during processing and evaluation.

Isolation of xenograft tumor RNA and expression profiling. NCI-H69 tumors were harvested for expression profiling 4 h after PDT treatment. Three treated tumors and three control untreated tumors, induced at the same time and of the same size, were independently harvested. The mice were killed using a Halothane overdose and the tumors were immediately flash frozen in liquid nitrogen. Samples were stored in RNAlater (Ambion) at ˉ80°C overnight, the tissue was then pulverized at liquid nitrogen temperature, and RNA was immediately isolated using Tri-reagent (Life Technologies) following the instructions of the manufacturer. Isolated RNA was stored at ˉ80°C till use.

RNA levels were determined by spectrophotometry, and RNA integrity was assessed using an Agilent 2100 bioanalyzer (Agilent). All samples scored at least 8/10 for overall integrity. The RNA samples extracted from the control and PDT-treated tumors was used to probe the Affymetrix GeneChip human genome array HG-U133A 2.0, which represents over 18,000 gene transcripts and variants including ~14,500 well-characterized human genes. cDNA amplification and synthesis of biotin-labeled cRNA were done with the one-cycle target labeling protocol using ~2 μg total RNA as described in the Affymetrix GeneChip Expression Analysis Technical Manual (March 2004). A total of 10 μg labeled and fragmented cRNA was hybridized to each chip. Washing and staining were done in the GeneChip Fluidics Station 450 using the Midi_euk2v3 protocol, and chips were scanned using an Affymetrix GeneChip Scanner 3000.

CEL file data have been submitted to the Gene Expression Omnibus (accession no. GSE8920). CHP and CEL files were imported into GeneSpring GX 7.3 (Agilent) for analysis. CEL files were normalized using Robust Multichip Averaging (32) with per chip and per gene median polishing. Flag data (present, marginal, or absent calls) was extracted from the CHP files, and data were filtered by both "present" calls and baseline raw signal intensity of at least 50 in at least three samples (equivalent of one condition). The resulting list was filtered for a modest fold change difference of 1.4 and subjected to ANOVA

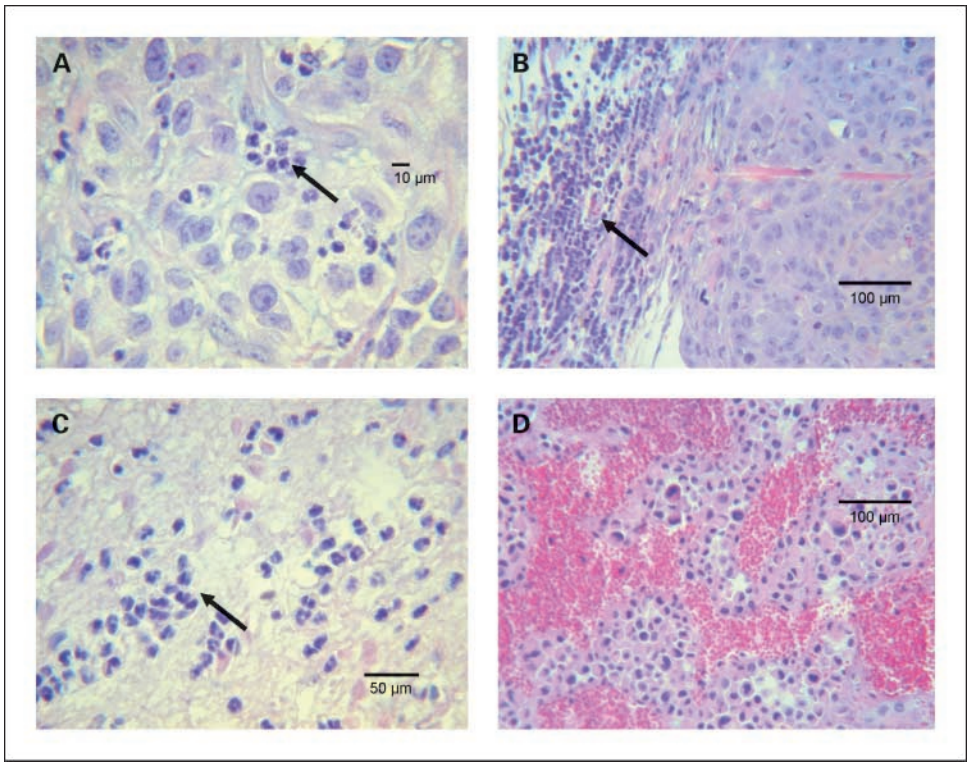

Fig. 3. Histology of PDT-treated tumors. *A,* a neutrophil infiltration (*black arrow*) in an A549 tumor that had started to regress. *B,* cells of the neutrophil/granulocyte lineage (*black arrow*) packed at the edge of an A549 tumor that had not started to regress. *C,* a neutrophil infiltration (*black arrow*) in a MDA-MB-231 tumor that had started to regress. *D,* an area of extensive vascular stasis and hemorrhage in a regressing MDA-MB-231 xenograft.

(Student's *t* test), resulting in a list of 124 statistically significant genes. The resulting genelist was further characterized using DAVID 2.0[7] (33), a program that creates and ranks functional categories according to the co-occurrence of annotation terms within a given genelist, drawing on descriptors from multiple annotation systems.

Expression of specific transcripts was also determined using real-time quantitative PCR. Total tumor RNA was isolated from PDT-treated and control NCI-H69 xenografts using the same techniques used to generate RNA samples for microarray profiling. RNA quality was assessed by analysis using an Agilent 2100 bioanalyzer, and only RNA with an integrity score of 8/10 or better was used for the real-time quantitative PCR experiments. Reverse transcription was conducted using the Ambion Retroscript kit with random decamer primers following the manufacturer's instructions. Amplification for specific products was then carried out using the SybrGreener kit from Invitrogen on a Corbette 3000 real-time PCR instrument. The majority of primers were designed using the Primer3 Web interface[8] and were synthesized by Integrated DNA Technologies. Commercial, verified primers for apoptotic markers were also obtained from Sigma and verified primers for β-actin were obtained from Real-time Primers. The primer sequences are given in Table 1. At the end of each amplification run, the melt profiles were generated for each amplicon to assess the quality of the target sequence amplification. Roto-Gene series 6000 software was used to quantitate the relative amounts of target sequence relative to β-actin.

Results

Linear and nonlinear spectroscopy of the new sensitizers. Figure 1C shows linear and nonlinear spectroscopic characteristics of the MPA79 sensitizer measured in organic solvents. The molar extinction spectrum (in methylene chloride; *inset a*) shows three main absorption peaks. Such features are characteristic of nonsymmetrical porphyrin-based constructs (29, 34) and correspond to the Soret band (430 nm) and two Q-bands (630 and 720 nm) of the core porphyrin. The 1PA peak of the bis(diphenylamino)distyrylbenzene chromophores occurs at 410 nm and overlaps with the intense Soret band at 430 nm. The long wavelength shoulder at about 470 nm has been shown to have strong charge-transfer character between the *m*-attached chromophores and the porphyrin core (34).

Figure 1C also shows a weak linear absorption at the far-red wing of the lowest-energy Q-band. Such absorption arises due to transitions from thermally activated vibrational levels in the ground electronic state (hot-band transitions; ref. 35).

The nonlinear femtosecond 2PA cross-section (in methylene chloride) increases steadily as the laser wavelength approaches the lowest energy Q-band. The shortest wavelength, at which the fluorescence intensity shows quadratic dependence on the laser pulse intensity, is 820 nm. The corresponding maximum intrinsic 2PA cross-section is $\sigma_2 \sim 1{,}500$ to 2,000 Goeppert-Mayer units. At wavelengths $\lambda_L < 820$ nm, the dependence gains an increasingly prominent linear component, indicating the onset of hot-band absorption. The quantum efficiency of singlet-oxygen generation for the targeted sensitizer used in this study (in toluene) was measured relative to H_2TPP (9) and was ~30% to 40%.

***Time course of targeted sensitizer uptake* in vitro.** Figure 2A shows that significant uptake took place for the SST2r-positive MDA-MB-231 cell line. A plateau was reached at 2 h and was maintained through 4 h. Based on our preliminary confocal microscopy studies of sensitizer-treated cells in culture, we know that the sensitizer is internalized in SST2r-positive cells (data

[7] http://david.abcc.ncifcrf.gov
[8] http://primer3.sourceforge.net

not shown). In contrast, only limited uptake of the targeted sensitizer was seen for the SST2r-negative CAPAN-1 cell line.

Regression response of PDT-treated tumors. Figure 1C shows the response of several human xenograft tumors to PDT treatment. All (100%) of the PDT-treated SCLC NCI-H69 xenografts exhibited excellent regression over the first week to 10 days. A few "cures" were noted (for instance, SCLC#1) where the tumor completely disappeared and did not regrow during the following 2 months of observation. However, the majority of the NCI-H69 xenografts did not completely regress and after a few weeks started to regrow. This was likely due to insufficient accuracy of aiming the rastering of the laser beam through the body of the mouse and also due to the fact that immunocompromised mice frequently fail to achieve cures after PDT treatment. Regressions, for instance NSCLC#1 in Fig. 2C, were also seen with the xenografts of the NSCLC A549 tumor, but only in 50% of the 10 such tumors treated (data not shown). No cures were observed for the A549 tumors. All 5 MDA-MB-231 xenografts, growing in the mammary fat pads and treated through the body of the mouse, also showed regressions over a similar time frame to the lung tumor xenografts. Two PDT-induced regressions for this human breast cancer cell line are also shown in Fig. 2C.

Gross and histopathologic appearance of PDT-treated tumors and control tissues. After laser irradiation, the area of the tumor xenograft became edematous. This condition persisted through the first day after treatment and had disappeared by 2 days after treatment. A black eschar was noted 1 day after treatment, and this persisted for the first week to 10 days after laser irradiation. When shed, this revealed normal freely mobile skin with no scaring. Normal hair regrew rapidly in the area, thereafter. Very little change was noted in the histology of either the untreated normal tissues or the normal tissues through which the laser beam passed. Normal tissues, harvested 24 to 48 h after PDT treatment of the xenograft, exhibited only minor vascular congestion in the lungs and

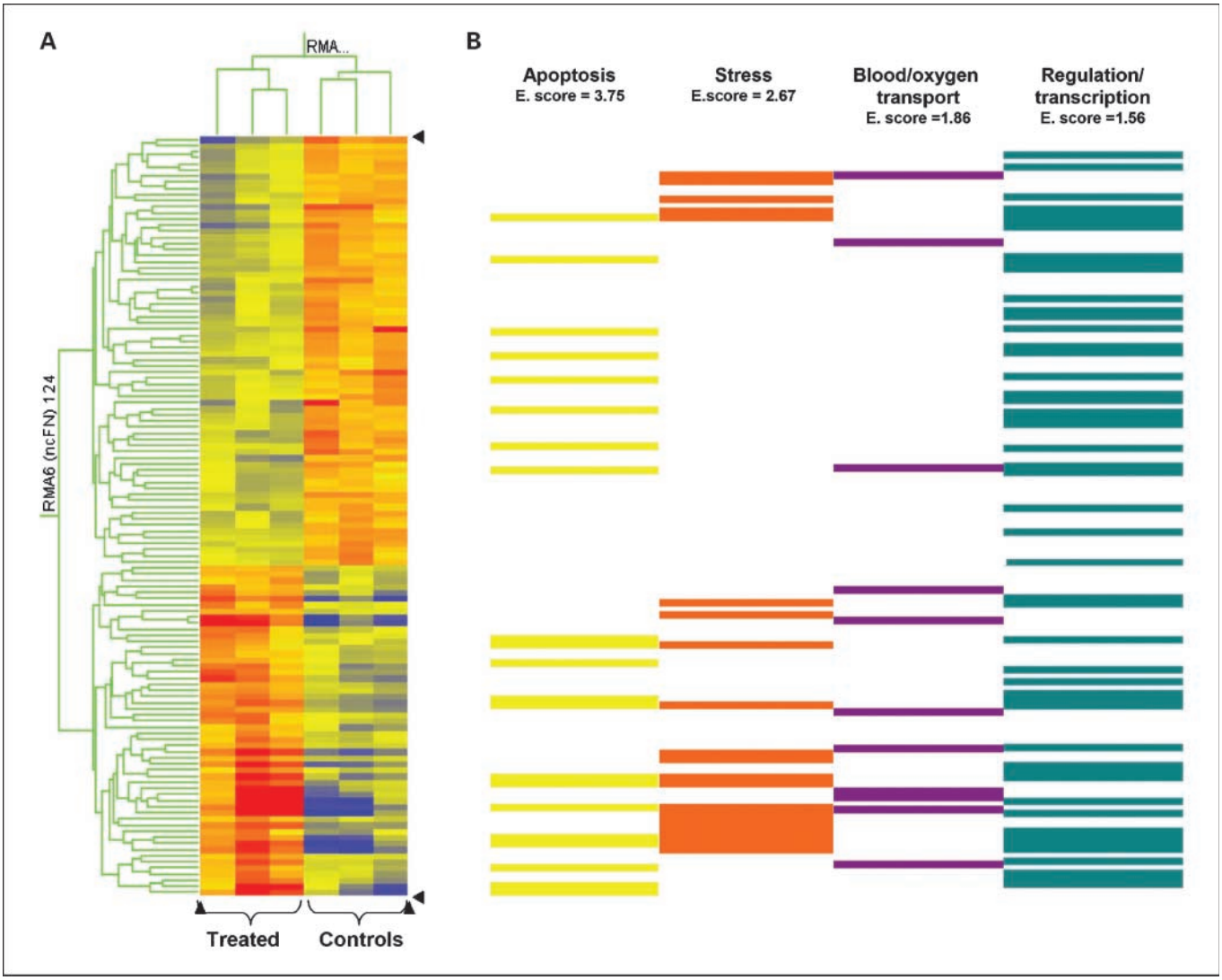

Fig. 4. *A,* a GeneSpring heat map for transcripts consistently altered in PDT-treated versus control NCI-H69 xenografts. *B,* DAVID "annotation" clusters for the same data. Both data sets are horizontally aligned.

slight edema in the wall of the intestine in the direct path of the laser (data not shown). PDT-treated tumors harvested during this time frame showed vascular stasis and hemorrhage that could be extensive (for instance, Fig. 3D). Tumor necrosis was also obvious, particularly in areas of vascular stasis and hemorrhage. PDT-treated tumor tissue harvested at the end of the first week after treatment showed an extensive infiltration of neutrophils (Fig. 3A and C) for those tumors, which were regressing. However, xenografts of the A549 NSCLC, which were not regressing, did not exhibit a neutrophil infiltration into the tumor tissue (Fig. 3B). Instead, less well differentiated cells of the same or similar lineage were seen packed around the periphery of the tumors (Fig. 3B).

Expression profiling of PDT-treated and untreated NCI-H69 xenografts. Excellent-quality RNA was isolated from both untreated tumors and tumors 4 h after PDT treatment. Using the GeneSpring program and a cutoff at 1.4-fold change, 124 genes were found to be consistently differentially expressed between PDT-treated and untreated tumors (Fig. 4). When the cutoff for fold change was raised to 2.0, this list dropped to 34. Several of the up-regulated transcripts deserve specific mention. As expected, an up-regulation of vascular endothelial growth factor was noted in treated tumors. The average fold increase was modest at 2.17 ($P = 0.02$) and probably resulted from oxygen depletion in the tumor region during treatment. The largest average fold increase was 30.25 ($P = 0.02$) for heat shock protein 70 (HSP70). Up-regulation of HSP70 is a canonical response to PDT treatment (6). These results also indicated an increase in average expression of apoptotic inducers such as Fos at 4.5-fold increase ($P = 0.003$; ref. 36) and Jun at 2.08-fold increase ($P = 0.03$; ref. 37). Transcripts for hemoglobin α2 (Hbα2) were on average 7.0-fold up-regulated ($P = 0.04$). This may have derived from remnant mRNA present in circulating reticulocytes in areas of vascular stasis and hemorrhage occurring in the PDT-treated tumors. Because the tumor vascular systems in these xenografts are of mouse origin, reticulocyte hemoglobin transcripts would also be murine. The hemoglobin gene is highly conserved between mouse and man with an 85% identity in amino acid sequence. Thus, it would not be surprising if its RNA hybridized to the human array. Alternatively, alveolar epithelial cells have been reported to express hemoglobin polypeptide transcripts (38), so the transcripts might also be of tumor cell origin.

The 124 transcripts showing ≥1.4-fold changes between PDT-treated and control tumors were then clustered using DAVID V 2.0, a program that clusters genes based on common annotation terms occurring in several different databases. Genes within the four significant annotation clusters from DAVID were matched in position to the GeneSpring heat map (Fig. 4B). By comparing the heat map with the DAVID cluster positions and identifying the specific gene functions, we noted that twice as many apoptosis-related genes were up-regulated in the PDT-treated tumors than were down-regulated. Of the apoptosis-related genes, over two-thirds were proapoptotic in character. A significant up-regulation in transcription of genes related to stress was also seen for PDT-treated over untreated tumors. Genes related to blood and oxygen transport were similarly up-regulated in PDT-treated tumors, as mentioned before, likely due to the vascular stasis and hemorrhage in the treated tumors. Many genes important to gene regulation and transcription showed changes in their expression levels between PDT-treated and control tumors. However, no specific patterns could be discerned.

The real-time quantitative PCR experiments run on the Corbette Rotogene, all generated a single amplicon with a melt-curve analysis inconsistent with primer dimers. No amplicon was obtained in the control assays lacking template. When compared with the results from Affymetrix GeneChips the fold increases for PDT-treated versus control NCI-H69 tumors assessed using quantitative PCR closely followed the same pattern. In both cases, the fold increases for HSP70 > Hbα > Fos > vascular endothelial growth factor. The fold increases were always somewhat higher for the Affymetrix GeneChips, but this could be related to the fact that different mouse groups were used for the two experimental protocols. The quantitative PCR results for Hbα were very similar (Table 1) whether primers designed from the human or the mouse sequence were used. This supports our contention that mouse transcripts for this gene would likely hybridize to the human Affymetrix GeneChip. The quantitative PCR experiments indicated small increases in Fos and Fas for treated tumors, whereas no changes for Bax and Bcl-2 were seen. Most likely, lack of changes in Bax and Bcl-2 reflected a very early stage in the apoptotic response to PDT treatment.

Discussion

Probably the greatest restriction in the current use of PDT is the limited tissue depth at which singlet oxygen can be generated. To provide a significant improvement in depth efficacy, light activation needs to be carried out in the NIR phototherapeutic window. By laser irradiating xenograft tumors through the bodies of host mice, we were able to document effective PDT at 2 cm of tissue depth. Furthermore, when such PDT-treated tumors were dye marked to facilitate recognition of their orientation, the gross changes associated with PDT damage were visible throughout the tumors even at the most distant regions of the tumor from the body surface of the mouse. Two centimeters is the maximal practical depth for treatment of tumors in mice. Because our PDT protocol did not appear to be limited by this depth, we feel that it is warranted to progress to larger animals, and we plan to conduct depth efficacy studies in spontaneous canine tumors. Tookad is the second generation sensitizer with the longest wavelength absorption peak at 763 nm, and it is under consideration for treatment of larger lung tumors and associated lung obstructions in human patients. Tookad PDT has been documented to lead to tumor necrosis at a depth of 1.3 cm for WISH-PC2 mouse xenografts (39) and to induce 3 cm diameter lesions in the canine prostate (40). The maximal depth efficacy of our new sensitizers is expected to be considerably more than that that indicated above. NIR tomography provides a much more linear pattern for tissue absorption than the currently used PDT activation sources, and it is likely that light penetration for PDT sources would drop off faster than for tomography. It has been estimated that NIR tomography could detect signals at as deep as 12 cm in the human breast (24). A conservative estimate for NIR PDT activation sources would therefore be a maximum penetration of 5 to 6 cm. This estimate would only hold for sensitizers with activation wavelengths that, unlike Tookad, lie well within the phototherapeutic

window. This maximal depth estimate is consistent with our earlier experiments, where we have shown that our sensitizers can be activated at a depth of at least 4 cm in tissue culture phantoms (data shown in Supplementary Materials).

Although the high-energy femtosecond pulsed laser was chosen to provide a sufficient photon flux to generate two-photon activation, such a laser should also produce less heating and phototoxicity such as conventional continuous wave, lower-energy medical lasers. The overall lack of laser-induced effects seen in the histology of normal tissues through which the laser beam passed supports the expected lack of phototoxicity. In addition, when we inserted a thermocouple probe into the tumor to measure tissue temperature during PDT activation, a maximal increase of only 7°C was detected (data not shown) and then only as the laser passed directly over the temperature probe. In comparison with recent studies of photothermal sensitization (41), our illumination has a much lower average release of thermal energy. We conclude that the heating, in itself, would be insufficient to cause the observed therapeutic effects.

The tumor regressions we observed were robust and followed the general pattern for post-PDT treatment found in the literature (39). When tumor regrowth occurred, in the majority of cases it started about 20 days post-treatment, also following the expected time frame. The mice were still in good condition at this point and could easily have withstood another PDT treatment. The histopathology of treated tumors was very similar to that reported by others for PDT treatment (39). The lack of neutrophil infiltration in A549 tumors that were not regressing at the time of sacrifice is interesting and suggests that there is a limiting factor acting on the granulocyte lineage. This could well be due to insufficient tumor damage occurring to stimulate up-regulation of complement genes, particularly C3a, thought to be major mediators of the post-PDT neutrophil response (5). A lesser PDT response would be expected for the A549 cell line that does not express SST2r and so should not internalize the sensitizer.

To the best of our knowledge, the expression profiling study reported in this article is the first to be carried out on PDT-treated tumors *in vivo*. Due to the requirement for excellent-quality RNA, we were constrained to harvest treated tumors before PDT killing became too well established. Thus, we were profiling the early response to this form of therapy. This could have contributed to signals too low for analysis for proinflammatory interleukins, where elevations in expression might have just been becoming established. Also, it would be expected that these would be predominantly mouse host responses. The degrees of homology for mouse versus human proinflammatory proteins is not high enough to expect the human microarray GeneChip to pick up the mouse transcripts well. There were no surprises in the list of 124 genes whose expression was consistently changed between untreated and PDT-treated tumors. An early apoptotic response appeared to be in place. We did see necrotic tissue in the histopathology studies, so it is likely that there was a mixed response. There have been several studies documenting up-regulation of various stress responses after PDT, and this DAVID cluster was to be expected. The possible lung tumor cell origin of Hbα polypeptide transcripts is interesting insofar as the expression is significantly elevated after PDT treatment. Recent reports of hemoglobin polypeptide expression in nonerythroid cells suggest a function for such expression in protection of cells from oxidative stress (38). Specifically, type II alveolar cells (38) and the A549 tumor cell line (38) have been shown to express hemoglobin transcripts. If increased expression of Hbα was a protective response to PDT treatment, this might contribute to the relative resistance to PDT treatment we noted for this tumor cell line. It was interesting that the human GeneChip array picked up changes for hemoglobin genes that were likely, at least partially, of mouse origin. These transcripts, however, have significant homology between species. To better analyze the inflammatory and immune host response, it would be useful to also run the extracted tumor RNAs against murine GeneChips.

One of the important advantages of PDT treatment of tumors is that it can induce a systemic antitumor immunity (6–8, 42). In this way, it is similar to thermal and cryotherapies (43–45). It has been shown that HSP70 released from PDT-treated cells has a key role in immune induction (6, 8) perhaps via activation of dendritic cells (42). PDT-induced cell lysates have been shown to be much more active than freeze/thaw tumor cell lysates in generating an antitumor response, and they contain much more HSP70 (8). A recent article by Kabingu et al. (7) has shown that PDT control of distant (untreated) tumors required a competent immune system, required natural killer cell activity, and led to persistent $CD8^+$ T-cell-mediated cytotoxicity. In attempts to improve this aspect of PDT treatment, several groups are now actively probing how to manipulate the immune system to enhance systemic antitumor immunity (8, 42).

Our choice of concentrating on human lung tumor xenografts was based on the fact that PDT is one of the treatment modalities being increasingly used for lung cancer, and it is approved for early NSCLC, a disease where many of the patients are inoperable at the time of diagnosis (1). For patients ineligible for surgery, PDT treatment can lead to good long-term survival, in one recent study giving a 72% complete response rate (46). PDT has also been used in combination with other modalities for induction therapy for NSCLC, with very encouraging results (47). Both SCLC and NSCLC have poor prognoses in part due to the high incidence of drug resistance (48). Therefore, there is considerable interest in the use of PDT, which is effective on drug-resistant tumors. Although, as indicated above, clinicians have started to use PDT during treatment of NSCLC, PDT sensitizers with greater-depth efficacy will be needed to effectively treat SCLC whose more rapid growth often leads to large tumors. There would be a considerable advantage for our new sensitizers in this environment. However, work still needs to be done on appropriate light delivery. We note that optical fibers capable of carrying high-peak intensity laser pulses are currently still only experimental (49).

Disclosure of Potential Conflicts of Interest

F. Meng, A. Gong, and C.W. Spangler are employed by MPA Technologies, Inc. C.W. Spangler received a commercial research grant from the Montana Board of Research Commercialization and Technology. J.R. Starkey received a commercial research grant from Rasiris, Inc., in which MPA Technologies has a minority ownership. C.W. Spangler, A.K. Rebane, and J.R. Starkey have between 5% and 35% ownership interests in MPA Technologies, Inc.

References

1. Triesscheijn M, Baas P, Schellens JH, Stewart FA. Photodynamic therapy in oncology. Oncologist 2006;9:1034–44.
2. Chen B, Pogue BW, Hoopes PJ, Hasan T. Vascular and cellular targeting for photodynamic therapy. Crit Rev Eukaryot Gene Expr 2006;16:279–305.
3. Sharman WM, Allen CM, van Lier JE. Role of activated oxygen species in photodynamic therapy. Methods Enzymol 2000;319:376–400.
4. Triesscheijn M, Ruevekamp M, Aalders M, Baas P, Stewart FA. Outcome of mTHPC mediated photodynamic therapy is primarily determined by the vascular response. Photochem Photobiol 2005;81:1161–7.
5. Stott B, Korbelik M. Activation of complement C3, C5, and C9 genes in tumors treated by photodynamic therapy. Cancer Immunol Immunother 2007;56:649–58.
6. Castano AP, Mroz P, Hamblin MR. Photodynamic therapy and anti-tumour immunity. Nat Rev Cancer 2006;6:535–45.
7. Kabingu E, Vaughan L, Owczarczak B, Ramsey KD, Gollnick SO. $CD8^+$ T cell-mediated control of distant tumours following local photodynamic therapy is independent of $CD4^+$ T cells and dependent on natural killer cells. Br J Cancer 2007;96:1839–48.
8. Bae SM, Kim YW, Kwak SY, et al. Photodynamic therapy-generated tumor cell lysates with CpG-oligodeoxynucleotide enhance immunotherapy efficacy in human papillomavirus 16 (E6/E7) immortalized tumor cells. Cancer Sci 2007;98:747–52.
9. Wilkinson F, Helman WP, Ross AB. Quantum yields for formation of singlet oxygen. J Phys Chem Ref Data 1993;22:113–262.
10. Kuimova MK, Hoffmann M, Winters MU, et al. Determination of the triplet state energies of a series of conjugated porphyrin oligomers. Photochem Photobiol Sci 2007;6:675–82.
11. Bhawalkar JD, Kumar ND, Zhao CF, Prasad PN. Two-photon photodynamic therapy. J Clin Laser Med Surg 1997;15:201–4.
12. Arnbjerg J, Johnsen M, Frederiksen PK, Braslavsky SE, Ogilby PR. Two-photon photosensitized production of singlet oxygen: optical and optoacoustic characterization of absolute two-photon absorption cross sections for standard sensitizers in different solvents. J Phys Chem A 2006;110:7375–85.
13. Oar M, Serin JM, Dichtel WR, Frechet JM, Ohulchanskyy TY, Prasad PN. Photosensitization of singlet oxygen via two-photon-excited fluorescence resonance energy transfer in a water-soluble dendrimer. Chem Mater 2005;17:2267–75.
14. Kim S, Ohulchanskyy TY, Pudavar HE, Pandey RK, Prasad PN. Organically modified silica nanoparticles co-encapsulating photosensitizing drug and aggregation-enhanced two-photon absorbing fluorescent dye aggregates for two-photon photodynamic therapy. J Am Chem Soc 2007;129:2669–75.
15. Karotki A, Khurana M, Lepock JR, Wilson BC. Simultaneous two-photon excitation of Photofrin in relation to photodynamic therapy. Photochem Photobiol 2006;82:443–52.
16. Collins HA, Khurana M, Moriyama EH, et al. Blood vessel closure using photosensitisers engineered for two-photon excitation. Nat Photonics 2008;2:420–4.
17. Moghissi K, Dixon K. Photodynamic therapy (PDT) in esophageal cancer: a surgical view of its indications based on 14 years experience. Technol Cancer Res Treat 2003;2:319–26.
18. Zoepf T, Jakobs R, Arnold JC, Apel D, Riemann JF. Palliation of nonresectable bile duct cancer: improved survival after photodynamic therapy. Am J Gastroenterol 2005;100:2426–30.
19. Canti G, Lattuada D, Morelli S, et al. Efficacy of photodynamic therapy against doxorubicin-resistant murine tumors. Cancer Lett 1995;93:255–9.
20. Chen B, Pogue BW, Hoopes PJ, Hasan T. Combining vascular and cellular targeting regimens enhances the efficacy of photodynamic therapy. Int J Radiat Oncol Biol Phys 2005;61:1216–26.
21. Schneider R, Tirand L, Frochot C, et al. Recent improvements in the use of synthetic peptides for a selective photodynamic therapy. Anticancer Agents Med Chem 2006;6:469–88.
22. Tremblay A, Leroy S, Freitag L, Copin MC, Brun PH, Marquette CH. Endobronchial phototoxicity of WST 09 (Tookad), a new fast-acting photosensitizer for photodynamic therapy: preclinical study in the pig. Photochem Photobiol 2003;78:124–30.
23. Cullander C. Light microscopy of living tissue: the state and future of the art. J Investig Dermatol Symp Proc 1998;3:166–71.
24. Srinivasan S, Pogue BW, Jiang S, et al. Interpreting hemoglobin and water concentration, oxygen saturation, and scattering measured *in vivo* by near-infrared breast tomography. Proc Natl Acad Sci U S A 2003;100:12349–54.
25. Schaer JC, Waser B, Mengod G, Reubi JC. Somatostatin receptor subtypes sst1, sst2, sst3 and sst5 expression in human pituitary, gastroentero-pancreatic and mammary tumors: comparison of mRNA analysis with receptor autoradiography. Int J Cancer 1997;70:530–7.
26. Taylor JE, Theveniau MA, Bashirzadeh R, Reisine T, Eden PA. Detection of somatostatin receptor subtype 2 (SSTR2) in established tumors and tumor cell lines: evidence for SSTR2 heterogeneity. Peptides 1994;15:1229–36.
27. Gulec SA, Drouant GJ, Fuselier J, et al. Antitumor and antiangiogenic effects of somatostatin receptor-targeted *in situ* radiation with (111)In-DTPA-JIC 2DL. J Surg Res 2001;97:131–7.
28. Nayak T, Norenberg J, Anderson T, Atcher R. A comparison of high- versus low-linear energy transfer somatostatin receptor targeted radionuclide therapy *in vitro*. Cancer Biother Radiopharm 2005;20:52–7.
29. Karotki A, Kruk M, Drobizhev M, Rebane A, Spangler CW. Efficient singlet oxygen generation upon two-photon excitation of new porphyrins with enhanced nonlinear absorption. IEEE J Selected Topics Quantum Electronics 2001;7:961.
30. Siehler S, Seuwen K, Hoyer D. ^{125}ITyr3octreotide labels human somatostatin sst2 and sst5 receptors. Eur J Pharmacol 1998;348:311–20.
31. Lamberts SW, Bakker WH, Reubi JC, Krenning EP. Somatostatin receptor imaging *in vivo* localization of tumors with a radiolabeled somatostatin analog. J Steroid Biochem Mol Biol 1990;37:1079–82.
32. Bolstad BM, Irizarry RA, Astrand M, Speed TP. A comparison of normalization methods for high density oligonucleotide array data based on variance and bias. Bioinformatics 2003;19:185–93.
33. Dennis G, Jr., Sherman BT, Hosack DA, et al. DAVID: Database for Annotation, Visualization, and Integrated Discovery. Genome Biol 2003;4:3.
34. Drobizhev M, Meng F, Rebane A, Stepanenko Y, Nickel E, Spangler CW. Strong two-photon absorption in new asymmetrically substituted porphyrins: interference between charge-transfer and intermediate-resonance pathways. J Phys Chem B 2006;110:9802–14.
35. Drobizhev M, Karotki A, Kruk M, Krivokapic A, Anderson HL, Rebane A. Upconversion fluorescence in porphyrins: one-photon hot-band absorption versus two-photon absorption. Chem Phys Lett 2003;370:690–9.
36. Luo X, Puig O, Hyun J, Bohmann D, Jasper H. Foxo and Fos regulate the decision between cell death and survival in response to UV irradiation. EMBO J 2007;26:380–90.
37. Cerezo-Guisado MI, Alvarez-Barrientos A, Argent R, Garcia-Marin LJ, Bragado MJ, Lorenzo MJ. c-Jun N-terminal protein kinase signalling pathway mediates lovastatin-induced rat brain neuroblast apoptosis. Biochim Biophys Acta 2007;1771:164–76.
38. Newton DA, Rao KMK, Dluhy RA, Baatz JE. Hemoglobin is expressed by alveolar epithelial cells. J Biol Chem 2006;281:5668–76.
39. Koudinova NV, Pinthus JH, Brandis A, et al. Photodynamic therapy with Pd-bacteriopheophorbide (TOOKAD): successful *in vivo* treatment of human prostatic small cell carcinoma xenografts. Int J Cancer 2003;104:782–9.
40. Chen Q, Huang Z, Luck D, et al. Preclinical studies in normal canine prostate of a novel palladium-bacteriopheophorbide (WST09) photosensitizer for photodynamic therapy of prostate cancers. Photochem Photobiol 2002;76:438–45.
41. El Sayed IH, Huang X, El Sayed MA. Selective laser photo-thermal therapy of epithelial carcinoma using anti-EGFR antibody conjugated gold nanoparticles. Cancer Lett 2006;239:129–35.
42. Saji H, Song W, Furumoto K, Kato H, Engleman EG. Systemic antitumor effect of intratumoral injection of dendritic cells in combination with local photodynamic therapy. Clin Cancer Res 2006;12:2568–74.
43. Fontana G, Pugliese A. The immune response to cryotherapy of prostatic carcinoma. G Batteriol Virol Immunol 1975;68:301–4.
44. Huang X, Jain PK, El Sayed IH, El Sayed MA. Determination of the minimum temperature required for selective photothermal destruction of cancer cells with the use of immunotargeted gold nanoparticles. Photochem Photobiol 2006;82:412–7.
45. Tanaka K, Ito A, Kobayashi T, et al. Heat immunotherapy using magnetic nanoparticles and dendritic cells for T-lymphoma. J Biosci Bioeng 2005;100:112–5.
46. Corti L, Toniolo L, Boso C, et al. Long-term survival of patients treated with photodynamic therapy for carcinoma *in situ* and early non-small-cell lung carcinoma. Lasers Surg Med 2007;39:394–402.
47. Ross P, Jr., Grecula J, Bekaii-Saab T, Villalona-Calero M, Otterson G, Magro C. Incorporation of photodynamic therapy as an induction modality in non-small cell lung cancer. Lasers Surg Med 2006;38:881–9.
48. Nadkar A, Pungaliya C, Drake K, Zajac E, Singhal SS, Awasthi S. Therapeutic resistance in lung cancer. Expert Opin Drug Metab Toxicol 2006;2:753–77.
49. Martynkien T, Szpulak M, Urbanczyk W. Modeling and measurement of temperature sensitivity in birefringent photonic crystal holey fibers. Appl Opt 2005;44:7780–8.

Clinical Cancer Research

New Two-Photon Activated Photodynamic Therapy Sensitizers Induce Xenograft Tumor Regressions after Near-IR Laser Treatment through the Body of the Host Mouse

Jean R. Starkey, Aleksander K. Rebane, Mikhail A. Drobizhev, et al.

Clin Cancer Res 2008;14:6564-6573.